Spectroscopic Study of Conformational Changes in Subdomain 1 of G-Actin: Influence of Divalent Cations

M. Nyitrai,* G. Hild,* J. Belágyi,# and B. Somogyi*
*Department of Biophysics and #Central Research Laboratory, University Medical School, Pécs H-7601, Hungary

ABSTRACT Temperature dependence of the fluorescence intensity and anisotropy decay of *N*-(iodoacetyl)-*N'*-(5-sulfo-1-naphthyl)ethylenediamine attached to Cys^{374} of actin monomer was investigated to characterize conformational differences between Ca- and Mg-G-actin. The fluorescence lifetime is longer in Mg-G-actin than that in Ca-G-actin in the temperature range of 5–34°C. The width of the lifetime distribution is smaller by 30% in Mg-saturated actin monomer at 5°C, and the difference becomes negligible above 30°C. The semiangle of the cone within which the fluorophore can rotate is larger in Ca-G-actin at all temperatures. Electron paramagnetic resonance measurements on maleimide spin-labeled (on Cys^{374}) monomer actin gave evidence that exchange of Ca^{2+} for Mg^{2+} induced a rapid decrease in the mobility of the label immediately after the addition of Mg^{2+}. These results suggest that the C-terminal region of the monomer becomes more rigid as a result of the replacement of Ca^{2+} by Mg^{2+}. The change can be related to the difference between the polymerization abilities of the two forms of G-actin.

INTRODUCTION

It is well established that actin can bind monovalent and divalent cations. There is a single high-affinity and at least three intermediate and lower affinity divalent-cation-binding sites in the monomer (G-actin) (see Estes et al., 1992, for a review). The high-affinity site is located in the cleft between the "small" and the "large" domains of actin monomer close to the nucleotide-binding site (Kabsch et al., 1990). Cation binding to the intermediate- or low-affinity binding sites results in a rapid conformational change (Rich and Estes, 1976; Carlier et al., 1986) that is thought to be the first step of the polymerization process, whereas a much slower conformational change occurs when Ca^{2+} is replaced by Mg^{2+} at the tight binding site (Frieden et al., 1980). The high-affinity binding site is occupied by Mg^{2+} in vivo in resting cells (Kitazawa et al., 1982), but in vitro it is usually occupied Ca^{2+} when the actin is prepared by standard procedures. The high-affinity binding site has different affinities for Ca^{2+} and Mg^{2+} (Strzelecka-Golaszewska and Drabikowski, 1968; Strzelecka-Golaszewska, 1973; Loscalzo and Reed, 1976; Strzelecka-Golaszewska et al., 1978), whereas the other sites do not greatly discriminate between these cations (Carlier et al., 1986). The binding of these metal ions to actin monomer at the high-affinity binding site can be adequately described with a simple competitive exchange model (Estes et al., 1987; Nowak et al., 1988; Selden et al., 1989; Gershman et al., 1991). Actin is a protein with one of the strongest known affinities for Ca^{2+} (in the nanomolar range) (Campbell, 1983); however, the cation on the high-affinity binding site is freely exchangeable (Kasai and Oosawa, 1968). The Ca^{2+} can be exchanged to Mg^{2+} in G-actin by the addition of the appropriate concentration of EGTA and $MgCl_2$ within 10 min (Strzelecka-Golaszewska et al., 1993). This procedure provides practically complete exchange and requires low Mg^{2+} concentration, which prevents polymerization.

Evidence has been accumulated that documents structural and functional differences between Ca- and Mg-actin (for a review, see, e.g., Estes et al., 1992; Carlier, 1990). Frieden and colleagues found that the fluorescent intensity of *N*-(iodoacetyl)-*N'*-(5-sulfo-1-naphthyl)ethylenediamine (IAEDANS) bound to the Cys^{374} residue of the actin monomer is sensitive to the cation content of the tight binding site, i.e., the intensity was increased by 10% as a result of Ca^{2+}-Mg^{2+} exchange (Frieden et al., 1980). This change can be taken as an indication of conformational differences between Ca- and Mg-G-actin. The conformational change in the actin monomer requires the presence of ATP (Frieden and Patane, 1985). According to the fluorescence measurements of Carlier and colleagues, the change that converts Ca-G-actin to a polymerizable species upon the addition of Mg^{2+} is associated with the binding of Mg^{2+} to the low-affinity sites and not with the exchange of Ca^{2+} for Mg^{2+} at the tight binding site (Carlier et al., 1986). The change in the steady-state fluorescence intensity has also been observed to be the result of the addition of Cd^{2+} or Mn^{2+} instead of Mg^{2+} (Zimmerle et al., 1987).

Actin saturated with Mg^{2+} has a critical concentration ~10 times lower and polymerizes faster than actin with bound Ca^{2+} (Kinosian et al., 1991). The in vitro polymerization of actin is accepted as a two-step process (nucleation and elongation, in that order). The two metal ions have different effects on different aspects of polymerization. Nucleation of Mg-actin is more efficient by many orders of magnitude than that of Ca-actin (Tobacman and Korn, 1983), whereas the elongation rates of Ca- and Mg-actin are similar (Gershman et al., 1989). The effects of the tightly

Received for publication 23 January 1997 and in final form 1 July 1997.
Address reprint requests to Dr. Bela Somogyi, Department of Biophysics, University Medical School, P.O.B. 99, Pécs H-7601, Hungary. Tel.: 36-72-314-017; Fax: 36-72-314-017; E-mail: sombel@apacs.pote.hu.

0006-3495/97/10/2023/10 $2.00

bound cations can be attributed to the differences in the mechanism and rate of ATP hydrolysis by F-actin (Carlier, 1990) (the rate of ATP hydrolysis is markedly higher when Mg^{2+} instead of Ca^{2+} is bound to the high-affinity site; Selden et al., 1990).

There is a continuous interest in understanding the conformational properties of the actin monomer that determining its ability to form filaments. This study is concerned with the difference in conformation and dynamics of the microenvironment around the Cys^{374} residue in the presence of different cations. The fluorescence intensity and anisotropy decay parameters of an extrinsic fluorophore (IAEDANS) covalently labeling the Cys^{374} residue of subdomain 1 were measured as a function of temperature in monomeric actin saturated with either Ca^{2+} or Mg^{2+}. The fluorescence quenching efficiency of an extrinsic, neutral quencher, the acrylamide, in both Ca- and Mg-G-actin was also measured. To corroborate the drawn conclusions, electron paramagnetic resonance (EPR) measurements were performed to monitor the change in the mobility of *N*-(1-oxyl-2,2,6,6-tetramethyl-4-piperidinyl)maleimide (MSL) spin label, which was covalently linked to the Cys^{374} residue of the actin monomer.

MATERIALS AND METHODS

Materials

KCl, $MgCl_2$, $CaCl_2$, tris-(hidroxy-methyl)amino-methane (Tris), acrylamide, glycogen, IAEDANS, MSL, and EGTA were obtained from Sigma Chemical Co. (St. Louis, MO). ATP and mercaptoethanol (MEA) were obtained from Merck (Darmstadt, Germany), and the NaN_3 was from FLUKA (Switzerland).

Protein preparation

Acetone-dried powder from rabbit skeletal muscle was obtained as described earlier (Feuer et al., 1948). Rabbit skeletal muscle actin was prepared according to the method of Spudich and Watt (1971), with a slight modification described by Mossakowska and colleagues (Mossakowska et al., 1988), and stored in 2 mM Tris-HCl (pH 8.0), 0.2 mM ATP, 0.1 mM $CaCl_2$, 0.1 mM MEA, and 0.02% NaN_3 (buffer A) for no longer than 2 days. Before fluorescence measurements, the G-actin solution was clarified by a 2-h ultracentrifugation at 100,000 × *g*. The concentration of G-actin was determined spectrophotometrically, using an absorption coefficient of 0.63 mg ml^{-1} cm^{-1} at 290 nm (Houk and Ue, 1974), with a Shimadzu UV-2100 spectrophotometer. A relative molecular mass of 42,300 Da was used for G-actin (Elzinga et al., 1973).

Fluorescence labeling of actin

Actin fluorescently labeled with IAEDANS at Cys^{374} was prepared according to the method of Miki and co-workers (Miki et al., 1987). F-actin (2 mg/ml in buffer A without MEA, supplemented with 0.1 M KCl and 2 mM $MgCl_2$) was incubated with a 10-fold molar excess of IAEDANS at room temperature for 1 h. The label was first dissolved in a few microliters of dimethylformamide (its final concentration in the labeling solution did not exceed 0.6% (v/v)) and then diluted ~50 times with the appropriate buffer before addition to the protein. After incubation the unreacted labels were removed by pelleting the actin by ultracentrifugation. The pellet was gently homogenized with a teflon homogenizer, and the homogenate was exhaustively dialyzed overnight against buffer A at 4°C. The concentration of the fluorescence dye in the protein solution was determined using the absorption coefficient of 6100 M^{-1} cm^{-1} at 336 nm for IAEDANS bound to actin (Hudson and Weber, 1973). The extent of labeling was determined to be 0.78–0.82 mol/mol of actin monomer.

Spin-labeling of actin

G-actin was polymerized by the addition of KCl and $MgCl_2$ to a final concentration of 100 mM and 2 mM, respectively. Actin was labeled in F-form with *N*-(1-oxyl-2,2,6,6-tetramethyl-4-piperidinyl)maleimide spin label (MSL) as described earlier (Mossakowska et al., 1988). One mole of spin label per mole of actin monomer was reacted for 90 min over ice. Unreacted labels were removed as described above. The degree of labeling varied between 0.2 and 0.55 mol/mol of actin.

Cation exchange in the actin monomer

Mg-G-actin was prepared from Ca-G-actin according to the method of Strzelecka-Golaszewska and colleagues (Strzelecka-Golaszewska et al., 1993). The protein solution was first diluted twofold with buffer A without $CaCl_2$ to decrease the concentration of Ca^{2+} to 50 μM. Then EGTA and $MgCl_2$ were added, to reach a final concentration of 0.2 mM and 0.1 mM, respectively, and the solution was incubated for 10 min at room temperature. The spectroscopic measurements were carried out within 50 min after the cation exchange.

Fluorescence lifetime and emission anisotropy measurements

Fluorescence lifetime and emission anisotropy decay were measured as a function of temperature in the range of 5–34°C. The concentration of actin was 23 μM. The fluorescence measurements were performed with an ISS K2 multifrequency phase fluorometer (ISS Fluorescence Instrumentation, Champaign, IL), using the frequency cross-correlation method. With this instrument, the phase delay and the demodulation of the sinusoidally modulated fluorescence signal were measured with respect to the phase delay and the demodulation of a standard reference substance (Fig. 1). Freshly prepared glycogen solution was used as a reference (lifetime = 0 ns). From these basic quantities the fluorescence lifetimes of the fluorophore were determined by nonlinear least-square analysis. In anisotropy decay measurements the sample was excited with polarized, sinusoidally modulated light. To resolve the anisotropy decay parameters, the difference between the phase angle and modulation ratio of the parallel and perpendicular components of the emission was used. The data were analyzed with ISS187 Decay Analysis software. The goodness of fit was determined from the value of the reduced χ^2 (Lakowicz, 1983a). This parameter was typically in the range of 0.5–2.5. The excitation light source was a 300-W Xe arc lamp. The excitation light intensity was modulated with a double-crystal Pockels cell. Excitation wavelength was set at 350 nm, and the emission was monitored through a KV 370 high-pass filter. The modulation frequency was changed in 10 steps (linearly distributed on a logarithmic scale) from 2 to 80 MHz and from 2 to 150 MHz in fluorescence lifetime and anisotropy decay measurements, respectively.

In fluorescence lifetime measurements, all data were fit to double-exponential decay curves or to unimodal Gaussian distribution, assuming a constant, frequency-independent error in both phase angle (±0.200°) and modulation ratio (±0.004). The same standard errors were used in anisotropy decay measurements as well. The uncertainty (standard error) associated with the parameters calculated using statistical analysis is given by the software (ISS187 Decay Analysis). The standard errors of parameters calculated by Eqs. 1, 4, 6, and 7 were obtained by the use of the law of error propagation. These standard errors probably underestimate the actual experimental uncertainties and therefore should be taken as the lower bound for the errors.

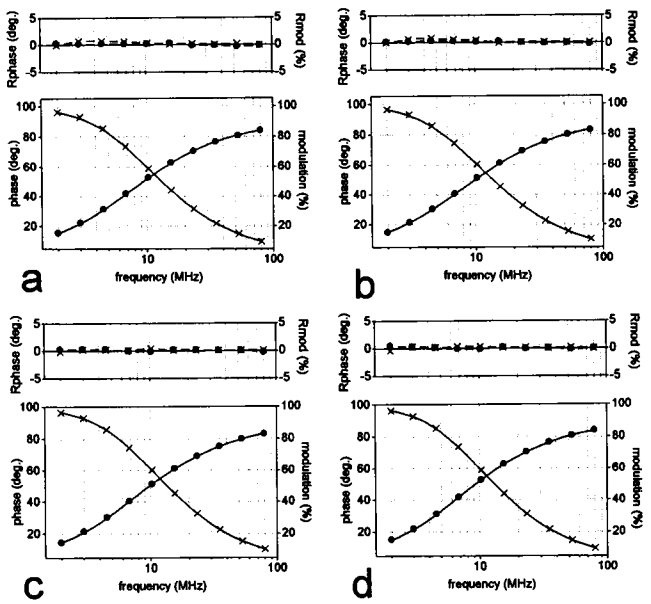

FIGURE 1 Representative plot of frequency-dependent phase (●) and modulation (+) values for the fluorescence intensity decay of IAEDANS in Ca-G-actin (*a,c*) and Mg-G-actin (*b,d*) at 15.1°C. The solid lines correspond to the unimodal Gaussian fits (*a,b*) or to two exponential fits (*c,d*). The difference between measured values and values calculated from the nonlinear least-squares fit can be seen on the upper panel.

In two-exponent lifetime analysis, the average fluorescence lifetimes were calculated as described by Lakowicz (1983a):

$$\tau_{aver} = (\tau_1^2\alpha_1 + \tau_2^2\alpha_2)/(\tau_1\alpha_1 + \tau_2\alpha_2) \quad (1)$$

where τ_{aver} is the average fluorescence lifetime, and α_i and τ_i are the individual amplitudes and lifetimes, respectively.

The anisotropy is expected to decay as a sum of exponentials (Belford et al., 1972). The raw data were fitted to a double-exponential function:

$$r(t) = r_1 \exp(-t/\varphi_1) + r_2 \exp(-t/\varphi_2) \quad (2)$$

where φ_1 and φ_2 are the two rotational correlation times with amplitudes r_1 and r_2, respectively. The limiting anisotropy recovered at zero time is given by

$$r_o = r_1 + r_2 \quad (3)$$

The two-dimensional angular range of the cone, Θ, within which the fluorophore wobbles, can be related to the amplitudes of the two rotational modes resolved in anisotropy decay measurements (Kinosita et al., 1977):

$$(r_1/(r_1 + r_2)) = (\cos^2\Theta(1 + \cos\Theta)^2)/4 \quad (4)$$

Here r_1 is the amplitude of the slower of the two exponential decay components.

The temperature-dependent fluorescence measurements were carried out with a thermostatted sample holder, which was flushed with dry air to avoid condensation. The temperature was maintained with a HAKE F3 water bath, and the temperature of the solution was continuously monitored in the sample holder.

Fluorescence quenching experiments

In quenching experiments, the fluorescence lifetime of IAEDANS was measured in the presence of different concentrations of acrylamide. Time-resolved experiments applied in our study have an advantage over the steady-state method in that the lifetimes at different quencher concentrations are only sensitive to dynamic quenching. To describe the dynamic quenching of fluorescence, the classical Stern-Volmer equation can be used (Lakowicz, 1983b):

$$\tau_o/\tau = 1 + K_{SV}[Q] \quad (5)$$

where K_{SV} is the Stern-Volmer quenching constant, τ_o is the lifetime of the fluorophore in the absence of quencher, and τ is the lifetime at different quencher concentrations [Q], and

$$K_{SV} = k_+\tau_o \quad (6)$$

where k_+ is the bimolecular rate constant characterizing the relative transport rate of the fluorophore and quencher molecules.

Light-scattering measurement

The intensity of the light scattered at 90° to incidence was measured on a Perkin-Elmer LS50B luminescence spectrometer. The concentration of the sample was 23 μM. The measurements were performed at 22°C. Both excitation and emission monochromators were set at 600 nm with optical slits of 3 nm.

EPR spectroscopy

EPR measurements were taken with a Bruker ESP 300E X-band spectrometer (Bruker A.G., Karlsruhe, Germany) at room temperature. For conventional 100-kHz field modulation (0.1–0.2 mT amplitude), a 10-mT field scan and 10-mW microwave power were used. The concentration of the samples in EPR measurements was 23 μM. Spectra were evaluated by the WIN-EPR program.

The order parameter, *S*, was calculated as proposed by Israelachvili and co-workers (Israelachvili et al., 1974):

$$S = \{[(3(A'_{11} - A_\perp))/(A_{11} - A_\perp)] - 1\}/2 \quad (7)$$

where A'_{11} is the outer hyperfine splitting measured in the experimental spectrum, $A_{11} \cong A_{ZZ}$ and $A_\perp = \frac{1}{2}(A_{XX} + A_{YY})$, where A_{XX}, A_{YY}, and A_{ZZ} are the principal values of the *A* tensor. The half-angle Θ can be obtained from the equation

$$S = (3\cos^2\Theta - 1)/2 \quad (8)$$

RESULTS AND DISCUSSION

It is well established that the conformation of monomer actin is sensitive to cation content (e.g., Estes et al., 1992; Carlier, 1990), but the characteristic feature of the difference between Ca- and Mg-G-actin is not clear. In our experiments, the measurements were performed over the temperature range of 5–34°C to characterize the fluorescence intensity and anisotropy decay of IAEDANS covalently linked to Cys^{374}. To further characterize this region, fluorescence quenching and EPR experiments were carried out as well.

The analysis of fluorescence lifetime measurements resulted in good fit, assuming either two discrete lifetime components or unimodal Gaussian lifetime distribution (Table 1 and Fig. 1). The appearance of two discrete components may assume two different populations of the fluorophore, which is usually thought to be determined by the physicochemical parameters of the environment. Previous

TABLE 1 The fluorescence lifetime of IAEDANS in Ca- and Mg-G-actin as a function of temperature

	Ca^{2+}-loaded G-actin						Mg^{2+}-loaded G-actin					
t (°C)	τ_1 (ns)	α_1	τ_2 (ns)	τ_{aver} (ns)	C (ns)	W (ns)	τ_1 (ns)	α_1	τ_2 (ns)	τ_{aver} (ns)	C (ns)	W (ns)
5.8	22.63	0.94	8.00	22.33	22.24	5.45	23.08	0.92	11.57	22.66	22.39	4.19
	(0.24)	(0.01)	(0.92)	(0.25)	(0.09)	(0.13)	(0.51)	(0.05)	(2.45)	(0.58)	(0.10)	(0.22)
9.6	22.25	0.93	8.28	21.87	21.68	5.48	22.13	0.97	6.61	22.01	22.05	4.58
	(0.26)	(0.02)	(0.86)	(0.27)	(0.09)	(0.12)	(0.18)	(0.01)	(1.14)	(0.18)	(0.09)	(0.18)
15.1	21.82	0.90	8.80	21.27	20.88	5.52	22.17	0.93	9.24	21.77	21.56	4.96
	(0.31)	(0.02)	(0.79)	(0.32)	(0.08)	(0.11)	(0.32)	(0.02)	(1.22)	(0.34)	(0.09)	(0.15)
22.7	19.96	0.93	6.48	19.64	19.50	5.51	20.76	0.94	6.91	20.47	20.00	5.10
	(0.14)	(0.01)	(0.48)	(0.14)	(0.08)	(0.09)	(0.21)	(0.01)	(1.05)	(0.21)	(0.08)	(0.10)
29.1	18.52	0.93	5.68	18.23	18.12	5.25	19.01	0.95	5.59	18.78	18.77	5.18
	(0.16)	(0.01)	(0.42)	(0.17)	(0.09)	(0.09)	(0.16)	(0.01)	(0.48)	(0.16)	(0.07)	(0.09)
33.7	17.68	0.93	5.44	17.41	17.35	5.07	19.08	0.89	7.36	18.53	18.06	5.16
	(0.16)	(0.01)	(0.42)	(0.16)	(0.08)	(0.08)	(0.53)	(0.02)	(0.53)	(0.18)	(0.07)	(0.08)

τ_i and α_i are the lifetimes and preexponential factors, respectively, assuming double-exponential decay, where $\alpha_1 + \alpha_2 = 1$. τ_{aver} is the average fluorescence lifetime (Eq. 3). C is the center and W is the width of the unimodal Gaussian distribution. The standard errors given by the analysis software are presented in parentheses.

analyses of fluorescence lifetime measurements based on the assumption of a discrete distribution resulted in the best fit, mostly with the use of two or a maximum of three exponential components. It seems to be unlikely that all of these investigated fluorophores have two different populations (different in fluorescence lifetime values); consequently, the case for the existence of two discrete components, which assumes two fluorophore populations, is not persuasive. To provide an alternative explanation of the heterogeneity of protein fluorescence, the distribution of fluorescence lifetime parameters was introduced (James and Ware, 1985; Engh et al., 1986; Alcala et al., 1987a–c; Gratton et al., 1988). It was shown that even if the physically veritable distribution is continuous, the analysis can still result in two or more discrete components (Demmer et al., 1987). Excluding the case where the two discrete lifetime components obviously belong to two different fluorophore populations, the only robust information from discrete analysis is the value of the average fluorescence lifetime. In addition to the average lifetime, one can obtain extra information by the use of continuous lifetime distribution. As has been shown (Alcala et al., 1987a–c; Gratton et al., 1988), the width of the distribution is related to the distribution and dynamics of the interconverting substates responsible for the appearance of lifetime distribution. In our experiments the average lifetime calculated from double-exponential analysis proved to be identical in each case, with the value of the center of the continuous lifetime distribution within the limits of the experimental error (Table 1). All of the above suggests that assuming a continuous lifetime distribution, at least in our case, where the mean values seem to be model independent, might give us a better approximation of the physical reality. Therefore, this kind of analysis will be discussed below.

The center value of the lifetime distribution of the IAEDANS emission is shorter in the presence of Ca^{2+} than in the presence of Mg^{2+} (Table 1), in agreement with the difference between the steady-state intensities measured for this fluorophore in Ca- and Mg-G-actin (Frieden et al., 1980). Below 30°C the width of the lifetime distribution is narrower in Mg-G-actin than that in Ca-G-actin, and the difference decreases with increasing temperature (Fig. 2), vanishing above 30°C.

The width of the lifetime distribution in Ca-G-actin is approximately constant below 25°C and decreases slightly at higher temperatures (Fig. 2). This tendency is not unusual, as reported earlier (Alcala et al., 1987a; Bismuto et al., 1988; Ferreira, 1989; Mei et al., 1992). Surprisingly, this parameter in Mg-G-actin increases with increasing temperature over the whole temperature range (Fig. 2). Two major processes are assumed to be responsible for the change in

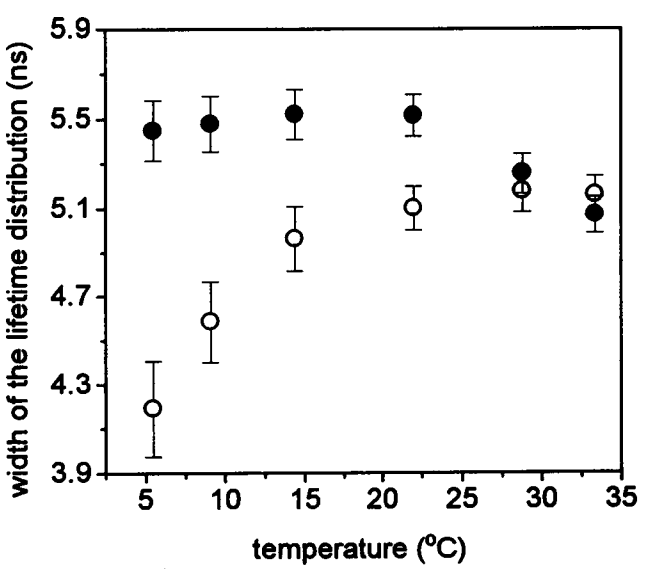

FIGURE 2 The width of lifetime distribution of the fluorescence of IAEDANS in Ca- (●) and Mg-G-actin (○).

the width of the lifetime distribution: the change in the number of populated substates and in the interconversion rate between substates may alter the value of this parameter. The interconversion rate is assumed to be faster at higher temperature, which would result in smaller width (Gratton et al., 1988; Ferreira and Gratton, 1990; Ferreira et al., 1994). Therefore, the increasing width of the distribution with increasing temperature in the case of Mg-G-actin is probably due to the increase in the number of populated substates of the fluorophore. In the case of Ca-G-actin, the change in the number of populated substates can also contribute to the temperature dependence of the width of lifetime distribution. Taking into account that the width of the distribution is approximately constant below 30°C (Fig. 2), it is very likely that in Ca^{2+}-loaded actin the number of populated substates is already relatively high, even at low temperatures. The effect due to the change in this number with increasing temperature is counterbalanced by the increase in the interconversion rate. Furthermore, the tendency in the change of the width of the lifetime distribution suggests that in Ca-G-actin the number of populated substates is higher at the lower temperature range compared to that number in Mg-G-actin. This might be the consequence of the looser structure of the C-terminal region in Ca^{2+}-saturated actin monomer.

To further characterize the conformational dynamics of subdomain 1, the rotational motion of IAEDANS was investigated by using anisotropy decay measurements over the 5–34°C temperature range. The analysis of the raw data of 12 independent measurements (Ca-G-actin and Mg-G-actin at different temperatures) showed that the decay is best described by two exponentials. The single-exponential fit to the raw data resulted in a χ^2 value of 37.1 ± 6.9. The assumption of two exponentials decreased this value to 2.3 ± 0.2, whereas the analysis assuming three exponential components did not further improve the value of χ^2 (2.12 ± 0.3). Therefore, in all cases, two rotational correlation times were used to fit the raw data (Table 2). The longer rotational correlation time decreases with increasing temperature in both Ca- and Mg-saturated actin monomer (Fig. 3). Our data are in good agreement with the measured values of Miki and co-workers (24.5 ns at 20°C) (Miki and Wahl, 1985). The longer rotational correlation times are also in agreement with the data of Ikkai and co-workers (Ikkai et al., 1979), who found φ_1 = 45 ns at 3.5°C for actin labeled with IAEDANS at Cys^{374} below the critical concentration. These values can be attributed to the overall rotational motion of the actin monomer. Furthermore, the anisotropy data indicate that both the Ca- and Mg-actin remained in monomer form during the measurements (Fig. 3).

To obtain more information about the microenvironment of Cys^{374}, a simple model was applied. To describe the hydrodynamic properties of the monomer actin, it is necessary to approximate its actual shape by a smooth and symmetrical geometrical figure. Among the simple figures that might serve as a good approximation of the monomer, the prolate ellipsoid and the sphere seem to be appropriate (Thomas et al., 1979; Montague et al., 1983). In the case of the prolate ellipsoid, the axial ratio is thought to be 1:1.5 or 1:2 (Montague et al., 1983; Kabsch et al., 1990). The rotation of the ellipsoid in general can be described by the use of three rotational correlation times. Using the axial ratios and assuming that the local rotational motion of the fluorophore is negligible, the ratio of these correlation times can be calculated (Lakowicz, 1991). If the axial ratio is 1:1.5, the calculation yields 1:0.94:0.80, whereas if the axial ratio of the prolate ellipsoid is assumed to be 1:2, the normalized correlation time values change to 1:0.87:0.63. These ratios are on the same order of magnitude, and because of the limitation of currently available fluorescence instrumentation, it is not possible to resolve the actual rotational correlation time values from anisotropy decay measurements (Lakowicz, 1991). Therefore, this limitation allows us to analyze the actin monomer by using only the spherical approximation.

Therefore the actin monomer is treated as a spherical protein that undergoes isotropic rotational diffusion in solution. The fluorophore with cylindrical symmetry is co-

TABLE 2 The anisotropy decay parameters of IAEDANS as a function of temperature in Ca- and Mg-G-actin

	Ca^{2+}-loaded G-actin				Mg^{2+}-loaded G-actin			
t (°C)	φ_1 (ns)	r_1	φ_2 (ns)	r_2	φ_1 (ns)	r_1	φ_2 (ns)	r_2
5.8	45.84	0.259	1.16	0.033	48.11	0.273	2.22	0.020
	(1.06)	(0.002)	(0.20)	(0.002)	(1.28)	(0.002)	(0.51)	(0.002)
9.6	44.01	0.236	2.14	0.041	43.79	0.263	2.94	0.024
	(1.35)	(0.003)	(0.25)	(0.003)	(1.39)	(0.003)	(0.63)	(0.003)
15.1	34.08	0.229	0.46	0.061	36.03	0.260	1.58	0.044
	(0.97)	(0.002)	(0.18)	(0.002)	(0.62)	(0.002)	(0.17)	(0.016)
22.7	27.53	0.213	0.98	0.073	30.43	0.232	1.84	0.054
	(0.90)	(0.002)	(0.16)	(0.003)	(0.60)	(0.003)	(0.15)	(0.002)
29.1	26.05	0.180	1.82	0.076	23.98	0.208	1.06	0.068
	(0.95)	(0.003)	(0.14)	(0.003)	(0.59)	(0.002)	(0.11)	(0.003)
33.7	25.33	0.161	1.68	0.096	26.43	0.175	1.56	0.084
	(1.00)	(0.003)	(0.10)	(0.002)	(0.92)	(0.003)	(0.11)	(0.002)

φ_i and r_i are the rotational correlation times and amplitudes, respectively. The standard errors given by the analysis software are presented in parentheses.

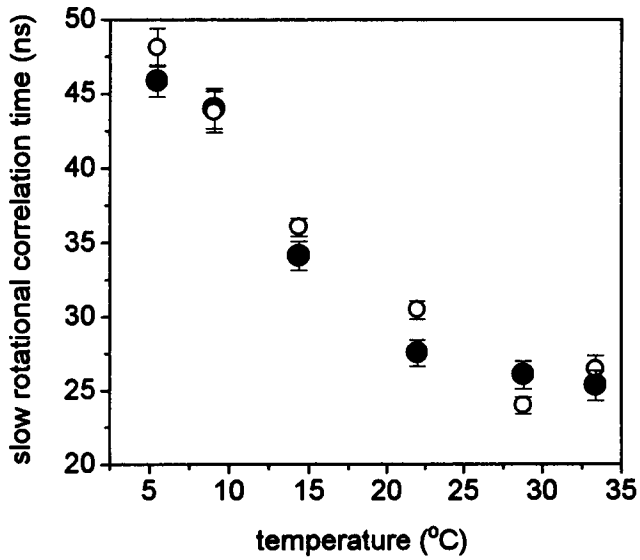

FIGURE 3 The slow rotational correlation time of the anisotropy decay of IAEDANS in Ca- (●) and Mg-G-actin (○).

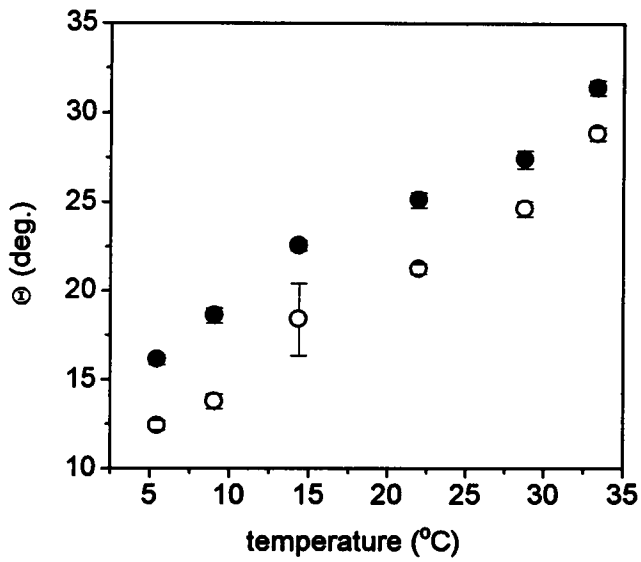

FIGURE 4 The calculated semiangles (Θ) of the cone within which the IAEDANS can rotate in Ca-G-actin (●) and Mg-G-actin (○).

valently attached to a specific site (Cys^{374}), and its symmetry axis is free to wobble through a limited angular range (within a cone of semiangle Θ). The rotational motion of the fluorophore is superimposed upon that of the whole protein. The longer rotational correlation time resolved in anisotropy decay measurements is attributed to the overall motion of the sphere-shaped protein, and the shorter one describes the wobbling of the fluorophore. Assuming that both the absorption and emission moments are parallel to the cylindrical axis of the fluorophore (Lipari and Szabo, 1980), the two-dimensional angular range, Θ, within which the fluorophore performs wobbling motion can be related to the amplitudes of the two rotational modes resolved in anisotropy decay measurements (Eq. 4). The use of this equation involves the assumption that the local motion of the label is much faster than the global motion of the protein, which seems to be reasonable, taking into account that the longer rotational correlation times are at least one order of magnitude larger than the shorter ones (Table 2).

The calculated semiangle (Θ) of the cone within which the fluorophore wobbles (see Eq. 4) is smaller in Mg-G-actin than in Ca-G-actin at all temperatures (Fig. 4).

The conventional EPR spectra of Ca- and Mg-G-actin are shown in Fig. 5. The spectrum of monomer actin always shows the superposition of spectra arising from labels that are bound to strongly and weakly immobilizing sites. The amount of the latter fraction is not more than 3–5%, indicating that the labeling procedure is highly selective: the labels are located on a single site, Cys^{374}.

The rotational correlation time for monomer actin was calculated in the conventional EPR time domain from the distance of the outer hyperfine extrema at ambient temperature and viscosity, and from the same distance measured at infinite viscosity (rigid limit). The hyperfine splitting constant changed from $2A'_{ZZ}$ = (6.305 ± 0.008) mT to 6.895 mT at room temperature as the viscosity increased. According to Goldman and co-workers (Goldman et al., 1972), φ_1 = 15.3 ns was calculated at room temperature and 1 mPas viscosity.

Replacing Ca^{2+} with Mg^{2+} resulted in an increased hyperfine splitting at a protein concentration of 23 μM, and the spectral parameter $2A'_{ZZ}$ attained a value of 6.645 ± 0.009 mT (φ_1 = 49 ns) after a lag phase of 30 min. At larger concentrations the lag phase decreased considerably. Partial polymerization of actin after the addition of Mg^{2+} cannot be

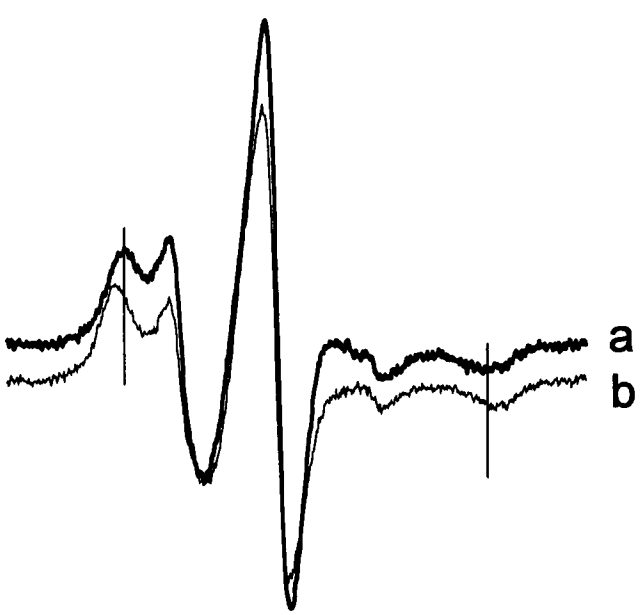

FIGURE 5 EPR spectra of MSL-labeled Ca- (*a*) and Mg-G-actin (*b*) (field scan: 10 mT). The spectrum of Mg-G-actin was recorded 15 min after the addition of 0.1 mM $MgCl_2$ and 0.2 mM EGTA to Ca-G-actin (23 μM).

excluded. When the samples were filtered through Millipore filters, which retained partially polymerized actin, the hyperfine splitting decreased to 6.424 mT (φ_1 = 20.8 ns). Assuming that the shape of the actin did not change significantly, it can be concluded that some rigidity exists around the labeled sites when the cation-binding site is occupied by Mg^{2+}.

The theoretical value of φ_1 was calculated to be 18.3 ns at room temperature, following Tao's formalism (Tao, 1969). This is in good agreement with the rotational correlation time recovered in our EPR experiments.

To compare the EPR and fluorescence data, the half-angle Θ was calculated from the EPR data as well. The restricted random-walk model within the confines of a cone was adopted (Jost et al., 1971), which allowed the calculation of a reasonable estimate of the half-angle Θ. The spectra of Mg-G-actin did not give resolved turning points from which one could estimate the inner splitting; therefore the calculation of the order parameter S proposed by Israelachvili and co-workers (Israelachvili et al., 1974) was used (Eq. 7); this is particularly useful in cases where the inner splitting is not measurable from experimental spectra.

Using the values A'_{ZZ} = (3.1225 ± 0.004) mT for Ca-G-actin and (3.269 ± 0.008) mT for Mg-G-actin, A_{II} = 3.5 mT, $A_{\perp}$ = 0.7 mT, the order parameters were S = (0.7978 ± 0.0086) for Ca-G-actin and (0.8763 ± 0.0177) for Mg-G-actin. The values of Θ were calculated (Eq. 8) to be 21.5° for Ca-G-actin and 16.7° for Mg-G-actin. Accordingly, the EPR data support the conclusions derived from fluorescence measurements, that the semiangle of the cone within which the reporter molecule undergoes diffusionlike motion is smaller in Mg-G-actin than in Ca-G-actin.

The inspection of the calculated parameters shows that both the longer rotational correlation time and the value of the cone half-angle are different from fluorescence anisotropy decay and EPR experiments. The differences probably arise from the difference between the fluorescence and EPR methods, which is not unusual according to earlier publications (e.g., Stryer, 1968). Furthermore, considering that different reporter molecules were used to study the protein matrix in the two methods, the difference in the mobilities of these labels might also contribute to the difference in the measured rotational correlation times and half-angles.

To study the effect of Mg^{2+} in the environment of Cys^{374}, the EPR signal was continuously monitored after the addition of Mg^{2+} (Fig. 6). The first spectrum was recorded 4 min after the preparation of Mg-G-actin. After a rapid increase, the splitting 2 A'_{ZZ} remained constant for a long time, but its value was different from that of F-actin. It was shown earlier that Mg^{2+} initially binds weakly, and this is followed by a conformational step resulting in tight Mg^{2+} binding, which is a prerequisite for the polymerization process (Frieden, 1983). Neutron scattering measurements revealed that magnesium induced slow formation of oligomers over a period of 12 h at 20°C at a Mg^{2+} concentration of 50 μM (Goddette et al., 1986). The rate of actin polymerization is strikingly dependent on the ionic

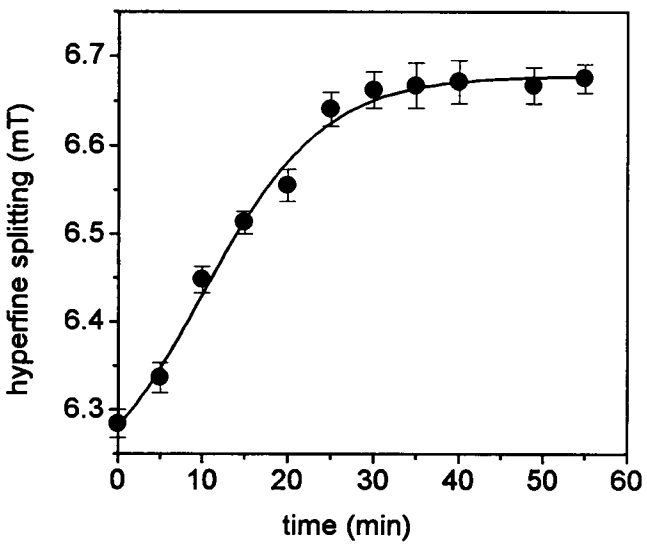

FIGURE 6 Plot of hyperfine splitting ($2A'_{zz}$) against time. Time was recorded after the addition $MgCl_2$ and EGTA to produce Mg-G-actin.

condition of solvent and concentration of actin. In these experiments, the actin concentration was low. In light scattering measurements, the intensity of the scattered light remained at a constant low level during the first 50 min after Ca^{2+}-Mg^{2+} exchange (data not shown). This might indicate that the nucleation-growth reaction is very slow (the addition of 100 mM KCl and 2 mM $MgCl_2$ (final concentrations) induced polymerization, which resulted in an eightfold increase in this low-level scatter intensity). Consequently, the EPR measurements indicate that the replacement of Ca^{2+} with Mg^{2+} at the high-affinity metal-binding site induces a conformational change in G-actin that leads to an increased rigidity in the environment of Cys^{374}.

According to the above conclusions, one may expect that the acrylamide quenching of the IAEDANS fluorescence would also give further evidence regarding the difference between Ca- and Mg-G-actin. In such experiments, the Stern-Volmer plots (τ_o/τ versus [Q]) proved to be linear in both Ca- and Mg-G-actin (Fig. 7), with a slight downward curvature appearing at higher quencher concentrations. The intercepts of the straight lines belonging to the plots are 1.04 ± 0.01 and 1.05 ± 0.01 for Ca-G-actin and Mg-G-actin, respectively, so the extent of the deviations from the theoretical value of 1.0 seems to fall within the range of the experimental error (the standard errors were given by the software used for linear regression). Therefore, the slopes of the straight lines (K_{SV}) were used to calculate the bimolecular quenching rate constant, k_+ (see Eq. 6). The values of k_+ ((1.0 ± 0.02) × 10^8 s^{-1} M^{-1} for Ca-G-actin and (1.2 ± 0.02) × 10^8 s^{-1} M^{-1} for Mg-G-actin) reflect a 20% increase in the quenching efficiency as a result of replacement of Ca^{2+} by Mg^{2+}. This observation indicates that the solvent accessibility of the fluorophore increases as a result of Ca^{2+}-Mg^{2+} exchange, which seems to be in conflict with the rest of our data presented here. Recent quenching data

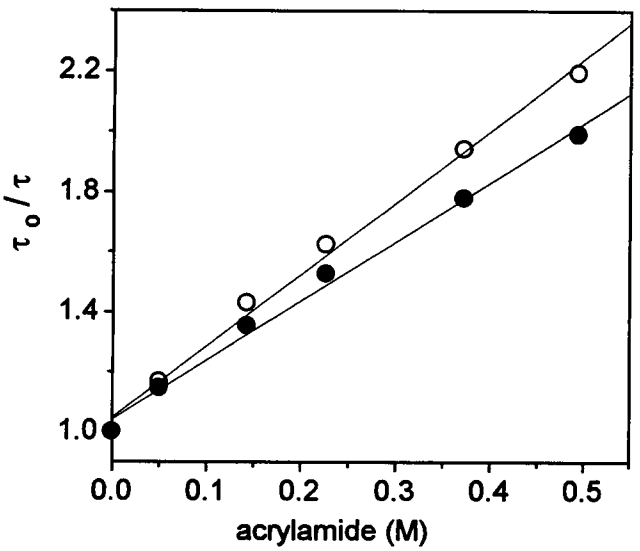

FIGURE 7 The Stern-Volmer plots for acrylamide quenching of IAEDANS fluorescence in Ca-G-actin (●) and Mg-G-actin (○).

show, however, that the interpretation of acrylamide quenching data is not straightforward. In some cases the quenching by penetrating acrylamide molecules can play a dominant role (Somogyi et al., 1994). Furthermore, proteins are able to bind acrylamide (Punyiczki et al., 1993; Matkó et al., 1980), and the bound acrylamide molecules can also contribute to the quenching. Given the fact that the bimolecular quenching rate constants we found are more than one order of magnitude smaller than those usually obtained for solvent-accessible fluorophores ($3–5 \times 10^9$ s^{-1} M^{-1}) (Eftink and Ghiron, 1976) one can conclude that clear interpretation of the acrylamide quenching data requires further study.

The substantial broadening of the lifetime distribution in Ca-G-actin compared to that value in Mg-G-actin below 30°C indicates that the fluorophore experiences a wider variety of microenvironments. The increase in the number of different microenvironments might be the consequence of the change in the rigidity of the protein segments. Therefore, the narrower distribution in the Mg^{2+}-loaded actin monomer below 30°C can be explained, in light of the EPR data, by the increased rigidity of the microenvironment in the vicinity of the fluorophore. The semiangle of the cone within which the reporter molecule can wobble is smaller in Mg-G-actin than that in Ca-G-actin. Apparently, when Ca- and Mg-G-actin are compared, the protein matrix in the C-terminal segment is more rigid when the actin is saturated with Mg^{2+}, and the structural elements form a more compact protein matrix, making the space for the tumbling of the external label smaller. This structural change might contribute to the enhancement of the nucleation step.

The change in the dynamics of subdomain 1 upon Ca^{2+}-Mg^{2+} exchange is in agreement with the suggestion of Strzelecka-Golaszewska and co-workers (Strzelecka-Golaszewska et al., 1993). They concluded from limited proteolytic digestion measurements that in G-actin the C-terminal segment becomes involved in some intramonomer interactions as a result of Ca^{2+}-Mg^{2+} exchange. Our results are also consistent with their conclusion that the presence of these intramonomer interactions in Mg-G-actin diminishes the accessibility of this segment.

Orlova and Egelman showed recently that the bending flexibility of filaments of Mg-actin is higher than that of filaments of Ca-actin (Orlova and Egelman, 1993). The different structural flexibility of actin filaments is attributed to the difference in either intermonomer bonding or intramonomer conformation and dynamics (Yanagida et al., 1984; Orlova and Egelman, 1992, 1993). Although it is difficult to interpret our spectroscopic data obtained on monomer actin forms in terms of the flexibility of actin filaments, it is very likely that the difference in the bending flexibility of the filaments of the Ca- and Mg-actin is not related to the difference in the C-terminal region of the protomer.

CONCLUSIONS

It was shown that the change in the cation content induces conformational change in the C-terminal domain of the actin monomer. Our data set suggests that subdomain 1 of actin monomer, or at least the local environment around the Cys^{374} residue in this subdomain, becomes more rigid when the Ca^{2+} is replaced by Mg^{2+}. Moreover, the smaller semiangle of the cone within which the reporter molecule can wobble in Mg-G-actin suggests that after the cation exchange the conformation of the C-terminal domain becomes less exposed to the solvent.

Subdomain 1 is one of the putative monomer-monomer binding sites in the polymerization process. The nucleation of the actin in the presence of Mg^{2+} is much faster than in the presence of Ca^{2+}, which can be attributed to the differences in the mechanism and rate of ATP hydrolysis (Carlier, 1990; Selden et al., 1990). It is possible, however, that the structural differences presented here also contribute to the faster nucleation process in Mg-actin. Taking into account that the C-terminal segment becomes more rigid as a result of Ca^{2+}-Mg^{2+} exchange, it is possible that the conformation of this region in Mg-G-actin provides better spatial conditions for other monomers to bind. This would explain why the major difference between Ca-G-actin and Mg-G-actin is limited to the difference in the nucleation rate (the elongation is practically insensitive to the ion content) (Tobacman and Korn, 1983).

This work was supported by grants from the National Research Foundation (OTKA grants T 017727, T 017099, and F 020174).

REFERENCES

Alcala, J. R., E. Gratton, and F. G. Prendergast. 1987a. Resolvability of fluorescence lifetime distributions using phase fluorometry. *Biophys. J.* 51:587–596.

Alcala, J. R., E. Gratton, and F. G. Prendergast. 1987b. Fluorescence lifetime distributions in proteins. *Biophys. J.* 51:597–604.

Alcala, J. R., E. Gratton, and F. G. Prendergast. 1987c. Interpretation of fluorescence decays in proteins using continuous lifetime distributions. *Biophys. J.* 51:925–936.

Belford, G. G., R. L. Belford, and G. Weber. 1972. Dynamics of fluorescence polarization in macromolecules. *Proc. Natl. Acad. Sci. USA.* 69:1392–1393.

Bismuto, E., E. Gratton, and G. Irace. 1988. Effect of unfolding on the tryptophanyl fluorescence lifetime distribution in apomyoglobin. *Biochemistry.* 27:2132–2136.

Campbell, A. K. 1983. Intracellular Calcium. John Wiley, Chichester. 91.

Carlier, M. F. 1990. Actin polymerization and ATP hydrolysis. *Adv. Biophys.* 26:51–73.

Carlier, M. F., D. Pantaloni, and E. D. Korn. 1986. Fluorescence measurements of the binding of cations to high-affinity and low-affinity sites on ATP-G-actin. *J. Biol. Chem.* 261:10778–10784.

Demmer, D. R., D. R. James, R. P. Steer, and R. E. Verrall. 1987. Three exponential fluorescence decay of horse liver alcohol dehydrogenase revealed by iodide quenching. *J. Photochem. Photobiol.* 45:39–48.

Eftink, M. R., and C. A. Ghiron. 1976. Fluorescence quenching of indole and model micelle systems. *J. Phys. Chem.* 80:486–493.

Elzinga, M., J. H. Collins, W. M. Kuehl, and R. S. Adelstein. 1973. Complete amino-acid sequence of actin of rabbit skeletal muscle. *Proc. Natl. Acad. Sci. USA.* 70:2687–2691.

Engh, R. A., L.-X. Chen, and G. R. Fleming. 1986. Conformational dynamics of tryptophan: a proposal for the origin of non-exponential fluorescence decay. *Chem. Phys. Lett.* 126:365–372.

Estes, J. E., L. A. Selden, and L. C. Gershman. 1987. Tight binding of divalent cations to monomeric actin. Binding kinetics support a simplified model. *J. Biol. Chem.* 262:4952–4957.

Estes, J. E., L. A. Selden, H. J. Kinosian, and L. C. Gershman. 1992. Tightly-bound divalent cation of actin. *J. Muscle Res. Cell Motil.* 13: 272–284.

Ferreira, S. T. 1989. Fluorescence studies of the conformational dynamics of parvalbumin in solution: lifetime and rotational motions of the single tryptophan residue. *Biochemistry.* 28:10066–10072.

Ferreira, S. T., and E. Gratton. 1990. Hydration and protein substates of proteins in reverse micelle. *J. Mol. Liq.* 43:253–272.

Ferreira, S. T., L. Stella, and E. Gratton. 1994. Conformational dynamics of bovine Cu, Zn superoxide dismutase revealed by time-resolved fluorescence spectroscopy of the single tyrosin residue. *Biophys. J.* 66: 1185–1196.

Feuer, G., F. Molnár, E. Pettkó, and F. B. Straub. 1948. Studies on the composition and polymerisation of actin. *Hung. Acta Physiol.* I:150–163.

Frieden, C. 1983. Polymerization of actin: mechanism of the Mg^{2+}-induced process at pH 8 and 20°C. *Proc. Natl. Acad. Sci. USA.* 80: 6513–6517.

Frieden, C., D. Lieberman, and H. R. Gilbert. 1980. Fluorescence probe for conformational changes in skeletal muscle G-actin. *J. Biol. Chem.* 255: 8991–8993.

Frieden, C., and K. Patane. 1985. Differences in G-actin containing bound ATP or ADP: the Mg^{2+}-induced conformational change requires ATP. *Biochemistry.* 24:4192–4196.

Gershman, L. C., L. A. Selden, H. J. Kinosian, and J. E. Estes. 1989. Preparation and polymerization properties of monomeric ADP-actin. *Biochim. Biophys. Acta.* 995:109–115.

Gershman, L. C., L. A. Selden, H. J. Kinosian, and J. E. Estes. 1991. High affinity divalent cation exchange on actin: association rate measurements support the simple competitive model. *J. Biol. Chem.* 266:76–82.

Goddette, D. W., E. C. Uberbacher, G. J. Bunick, and C. Frieden. 1986. Formation of actin dimers as studied by small angle neutron scattering. *J. Biol. Chem.* 261:2605–2609.

Goldman, S. A., G. V. Bruno, and J. H. Freed. 1972. Estimating slow-motional rotational correlation times for nitroxides by electron spin resonance. *J. Phys. Chem.* 76:1858–1860.

Gratton, E., N. Silva, and S. F. Ferreira. 1988. Fluorescence of tryptophan and protein dynamics. *In* Biological and Artificial Intelligence Systems. E. Clementi and S. Chin, editors. ESCOM Science Publishers, Leiden, The Netherlands. 49–56.

Houk, W. T., and K. Ue. 1974. The measurement of actin concentration in solution: a comparison of methods. *Anal. Biochem.* 62:66–74.

Hudson, E. N., and G. Weber. 1973. Synthesis and characterization of two fluorescent sulfhydryl reagents. *Biochemistry.* 12:4154–4161.

Ikkai, T., P. Wahl, and J. C. Auchet. 1979. Anisotropy decay of labeled actin. Evidence of the flexibility of the peptide chain in F-actin molecules. *Eur. J. Biochem.* 93:397–408.

Israelachvili, J., J. Sjösten, L. E. G. Ericsson, M. Ehrström, A. Graslund, and A. Ehrenberg. 1974. Theoretical analysis of the molecular motion of spin labels in membranes. *Biochim. Biophys. Acta.* 339:164–172.

James, D. R., and W. R. Ware. 1985. A fallacy in the interpretation of fluorescence decay parameters. *Chem. Phys. Lett.* 120:455–459.

Jost, P., L. J. Libertini, V. C. Hebert, and O. H. Griffith. 1971. Lipid spin labels in lecithin multilayers. Study of motion along fatty acid chains. *J. Mol. Biol.* 59:77–98.

Kabsch, W., H. G. Mannherrz, D. Shuck, E. F. Pai, and K. C. Holmes. 1990. Atomic structure of actin: DNase I complex. *Nature.* 347:37–44.

Kasai, M., and F. Oosawa. 1968. The exchangeability of actin bound calcium with various divalent cations. *Biochim. Biophys. Acta.* 154: 520–528.

Kinosian, H. J., L. A. Selden, J. E. Estes, and L. C. Gershman. 1991. Thermodynamics of actin polymerization: influence of the tightly-bound cation. *Biochim. Biophys. Acta.* 1077:151–158.

Kinosita, K., S. Kawato, and A. Ikegami. 1977. A theory of fluorescence polarization decay in membranes. *Biophys. J.* 20:289–305.

Kitazawa, T., H. Shuman, and A. Somlyó. 1982. Calcium and magnesium binding to thin and thick filaments in skinned muscle fibers: electron probe analysis. *J. Muscle Res. Cell Motil.* 3:437–454.

Lakowicz, J. R. 1983a. Measurement of fluorescence lifetimes. *In* Principles of Fluorescence Spectroscopy. Plenum Press, New York and London. 52–95.

Lakowicz, J. R. 1983b. Quenching of fluorescence. *In* Principles of Fluorescence Spectroscopy. Plenum Press, New York and London. 258–304.

Lakowicz, J. R. 1991. Topics in fluorescence spectroscopy. Principles. Plenum Press, New York and London. 1–22.

Lipari, G., and A. Szabo. 1980. Effect of librational motion on fluorescence depolarization and nuclear magnetic resonance relaxation in macromolecules and membranes. *Biophys. J.* 30:489–506.

Loscalzo, J., and G. H. Reed. 1976. Spectroscopic studies of actin-metal-nucleotide complexes. *Biochemistry.* 15:5407–5413.

Matkó, J., L. Trón, M. Balázs, J. Hevessy, B. Somogyi, and S. Damjanovich. 1980. Correlation between activity and dynamics of the protein matrix of phosphorylase b. *Biochemistry.* 19:5782–5786.

Mei, G., N. Rosato, N. Silva, Jr., R. Rusch, E. Gratton, I. Savini, and A. Finazzi-Agno. 1992. Denaturation of human Cu/Zn superoxide dismutase by guanidine hydrochloride: a dynamic fluorescence study. *Biochemistry.* 31:7224–7230.

Miki, M., C. G. dos Remedios, and J. A. Barden. 1987. Spatial relationship between the nucleotide-binding site, Lys-61 and Cys-374 in actin and a conformational change induced by myosin subfragment-1 binding. *Eur. J. Biochem.* 168:339–345.

Miki, M., and P. Wahl. 1985. Fluorescence energy transfer between points in G-actin: the nucleotide-binding site, the metal-binding site and Cys-374 residue. *Biochim. Biophys. Acta.* 828:188–195.

Montague, C., K. W. Rhee, and F. D. Carlson. 1983. Measurement of the translational diffusion constant of G-actin by photon correlation spectroscopy. *J. Muscle Res. Cell Motil.* 4:95–101.

Mossakowska, M., J. Belágyi, and H. Strzelecka-Golaszewska. 1988. An EPR study of the rotational dynamics of actins from striated and smooth muscle and their complexes with heavy meromyosin. *Eur. J. Biochem.* 175:557–564.

Nowak, E., H. Strzelecka-Golaszewska, and R. Goody. 1988. Kinetics of nucleotide and metal ion interaction with G-actin. *Biochemistry.* 27: 1785–1792.

Orlova, A., and E. H. Egelman. 1992. Structural basis for the destabilization of F-actin by phosphate release following ATP hydrolysis. *J. Mol. Biol.* 227:1043–1053.

Orlova, A., and E. H. Egelman. 1993. A conformational change in the actin

subunit can change the flexibilty of the actin filament. *J. Mol. Biol.* 232:334–341.

Punyiczki, M., J. A. Norman, and A. Rosenberg. 1993. Interaction of acrylamide with proteins in the concentration range used for fluorescence quenching studies. *Biophys. Chem.* 47:9–19.

Rich, S. A., and J. E. Estes. 1976. Detection of conformational changes in actin by proteolytic digestion: evidence for a new monomeric species. *J. Mol. Biol.* 104:777–792.

Selden, L. A., J. E. Estes, and L. C. Gershman. 1989. High affinity divalent cation binding to actin. *J. Biol. Chem.* 264:9271–9277.

Selden, L. A., L. C. Gershman, H. J. Kinosian, and J. E. Estes. 1990. Mg^{++} bound at the high affinity site is a cofactor for actin ATPase activity. *Biophys. J.* 57:325a.

Somogyi, B., M. Punyiczki, J. Hedstrom, J. A. Norman, F. G. Prendergast, and A. Rosenberg. 1994. Coupling between external viscosity and the intramolecular dynamics of ribonuclease T_1: a two-phase model for the quenching of protein fluorescence. *Biochim. Biophys. Acta.* 1209:61–68.

Spudich, J. A., and S. Watt. 1971. The regulation of rabbit skeletal muscle contraction. *J. Biol. Chem.* 246:4866–4871.

Stryer, L. 1968. Fluorescence spectroscopy of proteins. *Science.* 162: 526–533.

Strzelecka-Golaszewska, H. 1973. Relative affinities of divalent cations to the site of the tight calcium binding in G-actin. *Biochim. Biophys. Acta.* 310:60–69.

Strzelecka-Golaszewska, H., and W. Drabikowski. 1968. Studies on the exchange of G-actin-bound calcium with bivalent cations. *Biochim. Biophys. Acta.* 162:581–595.

Strzelecka-Golaszewska, H., J. Moraczewska, S. Y. Khaitlina, and M. Mossakowska. 1993. Localization of the tightly bound divalent-cation-dependent and nucleotide-dependent conformation changes in G-actin using limited proteolytic digestion. *Eur. J. Biochem.* 211:731–742.

Strzelecka-Golaszewska, H., E. Prochniewicz, and W. Drabikowski. 1978. Interaction of actin with divalent cations. 1. The effect of various cations on the physical state of actin. *Eur. J. Biochem.* 88:219–227.

Tao, T. 1969. Time-dependent fluorescence depolarization and Brownian rotational diffusion coefficients of macromolecules. *Biopolymers.* 8:609–632.

Thomas, D. D., J. C. Seidel, and J. Gergely. 1979. Rotational dynamics of spin-labeled F-actin in the sub-millisecond time range. *J. Mol. Biol.* 132:257–273.

Tobacman, L. S., and E. D. Korn. 1983. The kinetics of actin nucleation and polymerization. *J. Biol. Chem.* 258:3207–3214.

Yanagida, T., M. Nakase, K. Nishiyama, and F. Oosawa. 1984. Direct observation of motion of single F-actin filaments in the presence of myosin. *Nature.* 307:58–60.

Zimmerle, C. T., K. Patane, and C. Frieden. 1987. Divalent cation binding to the high- and low-affinity sites on G-actin. *Biochemistry.* 26: 6545–6552.